Bioresource Technology 454 (2026) 134711

Contents lists available at ScienceDirect

Bioresource Technology

journal homepage: www.elsevier.com/locate/biortech

New modelling approach for nitrogen transfer and water passage in gas-permeable membranes for wastewater treatment☆

A. Serra-Toro [a], T. Romero-Vidal [b], V. Pelizzaro [c], C. Da Silva [a], F. Valentino [c], S. Astals [a], J. Dosta [a,d,*], F. Mas [b,e]

[a] Department of Chemical Engineering and Analytical Chemistry, University of Barcelona, 08028, Spain
[b] Department of Materials Science and Physical Chemistry, University of Barcelona, 08028, Spain
[c] Department of Environmental Sciences, Informatics and Statistics, Ca' Foscari University of Venice, 30170 Mestre-Venice, Italy
[d] Water Research Institute, University of Barcelona, 08001, Spain
[e] Research Institute of Theoretical and Computational Chemistry (IQTCUB), University of Barcelona, 08028, Spain

HIGHLIGHTS

- New model captures ammonia and water transport across gas-permeable membranes.
- Total ammoniacal nitrogen diffusion is estimated using only measurable parameters.
- Method reliably models nitrogen recovery from synthetic and waste effluents.
- Consistent permeability of $1.3{\cdot}10^{-6}$ m/s confirms membrane-intrinsic behaviour.
- Water flux driven by osmotic gradients increases trapping volumes by up to 292%.

GRAPHICAL ABSTRACT

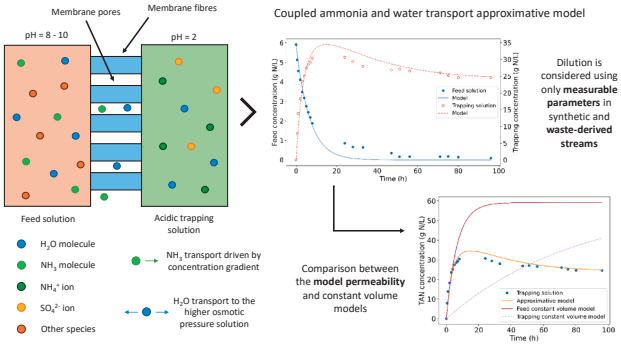

ARTICLE INFO

Keywords:
Biorefinery
Hydrophobic membranes
Nitrogen recovery
Osmotic distillation
Resource recovery

ABSTRACT

Gas-permeable membranes (GPM) have emerged as a promising technology for recovering total ammoniacal nitrogen (TAN) from wastewater. However, simultaneous transport of ammonia and water across hydrophobic membranes dilute the trapping solution and reduces its value. Additionally, water transport hinders nitrogen transfer analysis, which is used to assess membrane performance. Existing modelling approaches often rely on osmotic pressure estimates or assume constant volumes, which limits their applicability when treating real wastewaters. This study presents a new modelling approach to describe the coupled transport of ammonia and water across GPM using only experimentally measurable variables such as TAN concentration and solution volume. A key feature of this model is its capacity to capture dilution effects caused by water flux and accurately estimate TAN diffusion without requiring chemical speciation data. Laboratory experiments with synthetic and waste-derived effluents, including anaerobic digestion supernatant, acidogenic fermentation liquid, and industrial wastewater accurately reproduced TAN concentration over time. For synthetic wastewater, the mean ammonia permeability was $1.26{\cdot}10^{-6}$ m/s, while waste effluents showed broader values from $0.58{\cdot}10^{-6}$ to

☆ This article is part of a special issue entitled: 'IWA ecoSTP2025' published in Bioresource Technology.

* Corresponding author at: Department of Chemical Engineering and Analytical Chemistry, University of Barcelona, 08028, Spain.
E-mail address: jdosta@ub.edu (J. Dosta).

https://doi.org/10.1016/j.biortech.2026.134711
Received 22 January 2026; Received in revised form 22 April 2026; Accepted 22 April 2026
Available online 25 April 2026

$1.83 \cdot 10^{-6}$ m/s due to matrix component interactions. This narrow distribution confirms the robustness of the model, as permeability is a membrane-intrinsic parameter. Water transport significantly increased trapping solution volume, up to 149% in synthetic media and 292% in high-strength effluents, increasing with the osmotic pressure gradient between solutions. The proposed model provides a practical tool to obtain membrane-intrinsic ammonia permeability and to model TAN recovery in GPM treating real effluents, helping to bridge the gap between theoretical transport models and experimental applications.

1. Introduction

Human activities have drastically increased reactive nitrogen inputs to the environment, with nitrogen-rich wastewater discharges being a major driver of eutrophication, greenhouse gas emissions, and public health risks (Fowler et al., 2013). Concomitantly, global fertiliser demand is largely met through the highly energy intensive Haber-Bosch process, which accounts for about 2% of global energy consumption (Nancharaiah et al., 2016), and its demand continues to grow at an annual rate of 1.8% (Ledezma et al., 2015). Consequently, recovering ammoniacal nitrogen from wastewater serves a dual purpose of mitigating environmental impacts while contributing to the circular economy by valorising it as a valuable product (Qin et al., 2023). Recent reviews have highlighted source separation as a promising strategy to efficiently recover nitrogen in the form of usable fertiliser or chemical feedstock, with potential economic benefits estimated at 0.018–0.086 $/m^3 of treated wastewater (Errico et al., 2018; Qin et al., 2023).

A wide variety of biological and physicochemical processes have been proposed for ammoniacal nitrogen removal and recovery from residual effluents such as animal manure, agricultural digestates, and industrial waste streams (Rizzioli et al., 2023). Biological approaches, such as nitrification/denitrification and anammox, are widely applied to remove ammoniacal nitrogen from wastewater effluents at relatively low cost, although N_2O emissions should be carefully monitored and mitigated (Karmann et al., 2024). However, within the circular economy context, technologies that enable ammoniacal nitrogen recovery rather than removal should be prioritised, such as stripping, adsorption, ion exchange, and membrane-based processes, including forward osmosis and membrane distillation (Ye et al., 2018; Rizzioli et al., 2023). Each technology presents specific advantages and limitations with respect to energy demand, product quality, maintenance costs, and adaptability to complex matrices, among others (Farghali et al., 2024).

Among all these technologies, gas-permeable membranes (GPM) have emerged as a particularly promising technology for direct ammonia recovery. These hydrophobic membranes allow the diffusion of NH_3 through their gas filled nanopores or micropores into an acidic trapping solution where a concentrated ammonium salt solution is produced (García-González and Vanotti, 2015; Serra-Toro et al., 2024). Pilot and lab-scale studies have reported high total ammoniacal nitrogen (TAN) recovery efficiencies for the treatment of a wide range of feedstocks, including anaerobic digestion supernatant (Ferri da Silva et al., 2025), fermentation liquors (Serra-Toro et al., 2025), animal manure (González-García et al., 2021), or urine (Nagy et al., 2019). Furthermore, literature reviews have highlighted GPM as a low-energy and operationally versatile technology for economically valorising wastewater nitrogen (Soto-Herranz et al., 2022; Wu et al., 2026).

GPM technology still presents operational challenges that limit its robustness and durability, which are important factors for further scale-up of the technology. Strong osmotic pressure gradients between the feed and trapping solution can promote the passage of water molecules across the membrane via osmotic distillation, which dilutes the trapping solution and reduces process efficiency (Aligwe et al., 2020; Chan et al., 2020; Lee et al., 2021). Another phenomenon that contributes to water transport is membrane wetting, defined as the intrusion of liquid water through the membrane due to pore enlargement or loss of hydrophobicity (Wong et al., 2021). Wetting alters mass transfer mechanisms and facilitates small solutes transport across the membrane (Rongwong and Sairiam, 2020; Guo et al., 2022). In addition, fouling and pore clogging diminish the effective membrane surface, reducing its transfer rate and increasing the need for more frequent cleaning cycles (Ladewig and Al-Shaedi, 2017; Rosa e Silva et al., 2025). Understanding and quantifying the transport of both ammonia and water is essential to correctly interpret GPM performance. However, future research should focus on membrane degradation caused by wetting and fouling phenomena.

Developing reliable models that reflect the coupled transport and chemical effects governing ammonia transport is essential for interpreting GPM performance under variable conditions. Most existing modelling approaches simplify the process by assuming constant solution volumes or by neglecting the contribution of water transport across the membrane. When acid–base chemistry is incorporated in reaction–diffusion descriptions, the driving force for mass transfer remains the NH_3 concentration gradient, but the net TAN dynamics reflect the combined effect of diffusion and the NH_3/NH_4^+ equilibrium. Considering that acid–base kinetic is much faster than diffusive transport, the mass-transfer is linked to the intrinsic NH_3 permeability (P_{NH_3}) rather than a single empirical constant; typically expressed as the ammonia mass transfer constant (K_m) (Darestani et al., 2017; Reig et al., 2021; Serra-Toro., 2022a). However, when water transport occurs, dilution of the trapping solution can significantly influence the apparent TAN concentration dynamics, which may lead to inaccurate permeability estimations. This explains why K_m varies strongly with pH and temperature across different studies, while P_{NH_3} remains comparatively stable.

The model developed in this study incorporates water flux attributed to osmotic distillation but infers it only from measurable variables such as TAN concentration and solution volume, thereby avoiding the need for direct osmotic-pressure inputs. This aspect is particularly relevant when dealing with real wastewater matrices, where osmotic pressure and coefficients are often difficult to estimate due to the complex and variable composition of dissolved species. Despite recent advances in modelling ammonia transport in GPM, there remains a research gap in approaches that can reliably describe the coupled transport of ammonia and water without requiring detailed thermodynamic characterisation. The current study proposes a new modelling approach that describes the transport of both ammonia and water through GPM, remaining robust even when full speciation data are not available. By relying exclusively on experimentally measurable variables, the proposed model enables the interpretation of ammonia recovery processes under realistic conditions while explicitly accounting for dilution effects caused by water transport. As a result, the model provides a coherent and experimentally grounded framework for quantifying ammonia fluxes and dilution phenomena in GPM for waste-derived liquid streams.

2. Materials and methods

2.1. Synthetic solution and high-strength wastewaters

The synthetic solution consisted of deionised water with 5.0 g/L of acetic acid and different TAN concentrations: 2.4, 5.2, 7.1, and 10.6 g N/L. NH_4Cl was used as TAN source. Three different high-strength wastewater effluents were also tested to determine the performance of the GPM and the capability of the proposed model to predict the nitrogen diffusion and the water transport with real matrices. The first wastewater consisted of the supernatant from the anaerobic digestion (AD) effluent of the organic fraction of the municipal solid wastes (OFMSW)

collected from a full-scale mechanical–biological treatment plant in Barcelona. The second effluent was obtained in a mesophilic acidogenic fermentation process (35 °C), conducted in batch mode (7 days) with OFMSW influent to the aforementioned AD unit. The third effluent was wastewater collected from an animal by-product (ABP) processing facility. All wastewaters were sieved at 0.1 mm mesh size and centrifuged at 15000 × g for 10 min to remove suspended particles. Their characterisation is shown in Table 1, with TAN concentrations ranging between 5.7 and 9.9 g N/L.

2.2. Experimental set-up

The experimental system consisted of two sealed, jacketed glass tanks connected to a microporous hollow-fibre polypropylene membrane contactor with an active surface area of 0.50 m^2 (3 M, 1.7 × 5.5 MiniModule). A 5-L tank was used for the feed solution and a 3-L tank for the trapping solution (initially 0.1 M H_2SO_4) where TAN was recovered as $(NH_4)_2SO_4$. Both solutions were circulated in closed loops to the membrane module using a Masterflex L/S peristaltic pump, with flow rates of 15 L/h for the feed and 5 L/h for the trapping solution. Both tanks were hermetically sealed to prevent ammonia losses via volatilisation. A thermostatic bath (Thermo Scientific HAAKE DC30) was used to maintain a constant operating temperature of 35 °C in both tanks, since mesophilic conditions are largely utilised in biological processes and resulting effluents. Moreover, this temperature lies within the typical operational range reported for GPM systems and represents a compromise between efficient mass transfer and moderate operational costs (Zhu et al., 2024). Maintaining both solutions at the same temperature prevented the formation of temperature gradients across the membrane, which influence water transport and the interpretation of the transfer mechanisms (Varela-Corredor and Bandini, 2020). The feed circulated through the shell side of the membrane, while the trapping solution flowed through the lumen side to reduce the potential fouling. Each tank was equipped with a magnetic stirrer set at 180 rpm (Cimarec + basic 26 x 26, Thermo Scientific) and a pH control system. The pH was maintained at fix value of 2 and 9 in the feed and trapping solutions, respectively, using Crison electrodes (code 53–35) and controllers (pH 28). The controllers activated peristaltic pumps (Ismatec ISM827) to add an acidic (25% H_2SO_4) or alkaline solution (8 M KOH) as needed. Reagent consumption was added from a graduated cylinder and monitored to account for volume changes.

2.3. Experimental procedure

Several assays were performed changing the TAN concentrations of the synthetic solution (2.4, 5.2, 7.1, and 10.6 g N/L) and the feed-to-trapping volume relation (ω = 2 and 10) (Table 2). These factors affect the TAN concentration in the trapping solution, which in turn affect the water transport. The volume relation of 2 (ω = 2) was achieved by having a feed solution volume of 5.0 L and a trapping solution of 2.5 L, while experiments with ω = 10 had a trapping solution volume of 0.5 L. The experiments using synthetic wastewater with a volume relation of 10 (ω = 10) were obtained from published data in Da Silva et al. (2025). The volume relation used in tests with high-strength wastewaters varied (ω of 2, 5, and 10) depending on the wastewater tested, to ensure accurate assessment of water transport across the membrane (Table 2).

Table 1
Main characteristics of the studied waste-derived effluents.

Parameter (units)	OFMSW anaerobic digestion supernatant	OFMSW fermentation liquid	ABP wastewater
pH	8.2 ± 0.1	6.2 ± 0.1	7.2 ± 0.1
Conductivity (mS/cm)	50.6 ± 0.3	41.5 ± 0.2	57.9 ± 0.2
Soluble COD (g/L)	19.4 ± 1.9	54.6 ± 1.5	83.7 ± 3.4
VFA (g COD/L)	0.62 ± 0.01	30.9 ± 0.5	65.1 ± 3.6
Partial alkalinity (g $CaCO_3$/L)	20.7 ± 0.2	2.9 ± 0.2	10.2 ± 0.3
Total alkalinity (g $CaCO_3$/L)	24.0 ± 0.5	14.7 ± 0.5	33.7 ± 0.4
TAN (g N/L)	5.7 ± 0.1	6.1 ± 0.2	9.9 ± 0.3

Table 2
Experimental conditions of the tests carried out to assess the effect of TAN concentration and volume ratio (ω) on GPM performance.

Effluent	TAN (g N/L)	ω	Test
Synthetic wastewater	2.4	2	A1.1
		10	A2.1
	5.2	2	A1.2
		10	A2.2
	7.5	2	A1.3
		10	A2.3
	10.6	2	A1.4
		10	A2.4
OFMSW anaerobic digestion supernatant	5.7	2	B1
		10	B2
OFMSW fermentation liquid	6.1	2	C1
		10	C2
ABP wastewater	9.9	5	D

All experiments were carried out in duplicate. Nitrogen losses were evaluated by mass balance, with no significant losses detected. No significant changes in permeability values were observed among the experimental replicates, suggesting that fouling did not have a noticeable impact over the time scale of these experiments. Sampling was conducted over a 54-hour period. In the first 8 h, samples were taken hourly, with two samples collected in the first hour at 30-minute intervals. For overnight runs, samples were taken after 12 h and subsequently every 4 h. At each point, 4 mL were collected from both feed and trapping solutions and stored at 4 °C for TAN analysis. The volumes of both solutions were determined by measuring the liquid height in each chamber using a millimetre scale. The relationship between liquid height and volume had been previously calibrated, allowing the corresponding volumes to be obtained from the measured heights.

2.4. Analytical methods

Soluble COD was analysed using Method 5220C (APHA, 2017). TAN concentration was quantified with a Thermo Fisher Scientific ion-selective electrode (Orion 9512HPBNWP) according to Method 4500-NH3D (APHA, 2017). Alkalinity was measured using an automated titrator (Crison pH Burette 24) with 0.1 M HCl, following Method 2320B (APHA, 2017), and using a pH endpoint of 5.75 and 4.30 for the partial and total alkalinity, respectively. Volatile fatty acids (VFA), including acetic, propionic, butyric, valeric, and caproic acids, were quantified using a Shimadzu GC-2010 Plus gas chromatograph equipped with a DB-FFAP capillary column and a flame ionisation detector. VFA concentrations were converted to COD equivalents using theoretical conversion factors: 1.07 (acetic), 1.51 (propionic), 1.82 (butyric), 2.04 (valeric), and 2.21 mg COD/mg compound (caproic acid).

2.5. Model description

A novel approach describing the transport of TAN across GPM in real wastewater matrices was built upon the modelling framework proposed by Da Silva et al. (2025). The proposed methodology enables the quantification of ammonia permeability under conditions where osmotic pressure and osmotic coefficients are either unavailable or experimentally difficult to determine. The variables used in equations (1), (2) and (3) are defined as follows:

$$TAN_i(t) = \frac{m_{TAN,i}(t)}{V_i(t)} \quad (1)$$

$$m_{TAN,i}(t) = mNH_{3,i}(t) + mNH_{4,i}^{+}(t) \tag{2}$$

$$n_{TAN,i}(t) = nNH_{3,i}(t) + nNH_{4,i}^{+}(t) \tag{3}$$

Where *TAN* denotes the total ammoniacal nitrogen concentration (g N/L), with the subscript *i* referring to either the feed (f) or the trapping (t) solution. $V_i(t)$ represents the volume of compartment *i*, which may vary over time due to transmembrane water flux (L). Parameters $m_{TAN,i}(t)$ and $n_{TAN,i}(t)$ correspond to the TAN expressed in mass (g) and molar (mol) units, respectively. The mass and molar units are inherently correlated through the molar mass of nitrogen species, equation (4) describes the proportional relation to their initial values in the feed solution.

$$\frac{m_{TAN,i}(t)}{m_{TAN,f}(0)} = \frac{n_{TAN,i}(t)}{n_{TAN,f}(0)} \tag{4}$$

The chemical equilibrium between ammonia (NH_3) and ammonium ion (NH_4^+) is governed by the acid–base dissociation reaction. Given the rapid kinetics of this equilibrium, it could be assumed that acid–base equilibrium is always established on both sides of the membrane. The equilibrium condition, expressed in equation (5), relates the concentrations of the species via the acid dissociation constant K_a, assuming ideal conditions and approximating activities to both species concentration. Equations (6), (7) and (8) represent the proportion of NH_3, the species capable to diffuse through the membrane, depending on the pH and temperature.

$$K_a \approx \frac{\left[NH_{3,i}(t)\right]\cdot a_{H^+}}{\left[NH_{4,i}^{+}(t)\right]} = \frac{nNH_{3,i}(t)\cdot 10^{-pH_i}}{nNH_{4,i}^{+}(t)} = 10^{-pK_a} \tag{5}$$

$$nNH_{4,i}^{+}(t) = nNH_{3,i}(t)\cdot 10^{pK_a - pH_i} = \mu_i\, nNH_{3,i}(t)\ ;\ \mu_i \equiv 10^{pK_a - pH_i} \tag{6}$$

$$n_{TAN,i}(t) = (1+\mu_i) nNH_{3,i}(t); nNH_{3,i}(t) = \frac{n_{TAN,i}(t)}{(1+\mu_i)} \tag{7}$$

Equation (7) could also be expressed in mass units from equation (4), as stated in equation (8).

$$m_{TAN,i}(t) = (1+\mu_i) mNH_{3,i}(t); mNH_{3,i}(t) = \frac{m_{TAN,i}(t)}{(1+\mu_i)} \tag{8}$$

Temperature variation of the dissociation equilibrium constant (K_a) is given by van't Hoff's equation:

$$\frac{dlnK_a}{dT} = \frac{\Delta H^{\circ}}{RT^2}; K_a = exp\left(-\frac{6334}{T}\right) \tag{9}$$

Where *T* denotes the absolute temperature (K), ΔH° is the standard enthalpy of the reaction (J/mol) and *R* is the universal gas constant. The integrated expression is obtained by assuming that ΔH° remains constant around the operating temperature of 35 °C.

The TAN transport is governed by mass balance equations, while the diffusion of TAN is controlled by the chemical potential gradient of NH_3 in solution, which, assuming ideal conditions, is equivalent to a concentration gradient (equation (10)). Due to the pH difference and membrane selective permeability, NH_3 diffuses through the membrane, whereas NH_4^+ is retained. Consequently, the transport model may be simplified and expressed either in molar or mass form (equation (10)).

$$\begin{aligned}\frac{dn_{TAN,f}(t)}{dt} &= \left(\frac{d\left(nNH_{3,f}(t)\right)}{dt} + \frac{d\left(nNH_{4,f}^{+}(t)\right)}{dt}\right)\\ &= A\,P_{NH_3}\left(\frac{nNH_{3,t}(t)}{V_t(t)} - \frac{nNH_{3,f}(t)}{V_f(t)}\right)\\ &= A\,P_{NH_3}\left(\frac{n_{TAN,t}(t)}{(1+\mu_t)V_t(t)} - \frac{n_{TAN,f}(t)}{\left(1+\mu_f\right)V_f(t)}\right)\end{aligned} \tag{10}$$

Where P_{NH_3} (m/s) is the permeability of NH_3 across the membrane and *A* (m^2) is the membrane surface area. Provided that pH in the trapping solution is always acidic (below 5), the ammonia fraction in the solution is assumed to be negligible and thus, a general equation from the previous balance is obtained (equation (11)).

$$\frac{dm_{TAN,f}(t)}{dt} = -\frac{A\,P_{NH_3}}{\left(1+\mu_f\right)}\frac{m_{TAN,f}(t)}{V_f(t)} = -\frac{A\,P_{NH_3}}{\left(1+\mu_f\right)}TAN_f(t) \tag{11}$$

In the limiting case where transmembrane water flux is negligible, both solution volumes are treated as constant. The resulting equation under such assumptions is presented in equation (12) and the general solution, either in mass or in concentration, is shown in equation (13).

$$\frac{dm_{TAN,f}(t)}{dt} = -\frac{A\,P_{NH_3}}{\left(1+\mu_f\right)}\frac{m_{TAN,f}(t)}{V_f} \tag{12}$$

$$\begin{aligned}m_{TAN,f}(t) &= m_{TAN,f}(0)\,exp\left(-\frac{A\,P_{NH_3}}{\left(1+\mu_f\right)V_f}t\right) \quad ; \quad TAN_f(t)\\ &= TAN_f(0)\,exp\left(-\frac{A\,P_{NH_3}}{\left(1+\mu_f\right)V_f}t\right)\end{aligned} \tag{13}$$

In most GPM studies, where only NH_3 diffuses through the membrane, the TAN mass balance is simplified. The acid–base equilibrium is not explicitly considered since the feed is usually maintained under alkaline conditions. As a result, TAN depletion is only attributed to NH_3 diffusion across the membrane, and the integrated expression assumes that its variation directly reflects NH_3 mass transfer. Under this assumption, the exponential term of equation (13) includes an apparent mass-transfer coefficient K_m, without the equilibrium correction factor μ, which depends on pH and temperature (equation (6)).

When acid–base reactions are explicitly included, as in reaction–diffusion models, the driving force for transport remains the NH_3 concentration gradient. However, the overall TAN variation depends on both diffusion and acid–base kinetics. The acid-base reactions are much faster than the diffusion process and can therefore be assumed to be at equilibrium. Consequently, the integrated expression includes $P_{NH_3}/(1+\mu_f)$ instead of a simple K_m. Accordingly, K_m should be interpreted as an apparent mass-transfer coefficient dependent on the intrinsic permeability P_{NH_3} as well as on pH and temperature. This explains why K_m ($TAN \propto \exp(A \cdot K_m \cdot t/V_f)$) vary by orders of magnitude under different operating conditions, while P_{NH_3} remains comparatively stable. This interpretation bridges the simplified empirical formulations commonly used in GPM studies (Darestani et al., 2017; Reig et al., 2021; Serra-Toro et al., 2022b) with more rigorous equilibrium–diffusion models.

The chamber volumes become time dependent in those scenarios involving water flux across the membrane. Consequently, the governing dimensional equation takes the form of an ordinary differential equation (ODE) (equation (13)). Its solution cannot be obtained analytically because the evolution of the feed volume ($V_f(t)$) and mass of TAN ($m_{TAN,f}(t)$) are interdependent, being coupled through the osmotic pressure gradient across the membrane.

An approximate analytical solution was employed to decouple the

water flow driven by the osmotic pressure gradient from the TAN flux, since measuring the osmotic pressure in wastewater systems is difficult or cannot be accurately estimated due to unknown solute composition and osmotic coefficients (Greisner et al., 2023). This approximation assumes an exponential decay in the feed TAN concentration and permits direct fitting of the experimental data (Da Silva et al., 2025. The assumption is supported by previous models and literature, where solute depletion over time is described by a negative exponential function due to first order-like transport behaviour (Serra-Toro et al., 2022a):

$$TAN_f(t) \approx TAN_f(0)exp(-a_{exp}t) \tag{14}$$

Then, equation (12) becomes a non-homogeneous ordinary differential equation (ODE).

$$\frac{dm_{TAN,f}(t)}{dt} = -\frac{AP_{NH_3}}{(1+\mu_f)}TAN_f(0)exp(-a_{exp}t) \tag{15}$$

Whose analytical solution can be obtained using the method of separation of variables, by knowing the initial TAN mass value ($m_{TAN}(0)$).

$$m_{TAN,f}(t) = m_{TAN,f}(0)\left(1 - \frac{A\,P_{NH_3}}{(1+\mu_f)V_f(0)}\frac{1}{a_{exp}}\left[1 - exp(-a_{exp}t)\right]\right) \tag{16}$$

The expression for a_{exp} (equation (17)) can be obtained from equation (16) assuming that TAN concentration in the feed solution tends to zero as time approaches infinite.

$$m_{TAN,f}(0)\left(1 - \frac{A\,P_{NH_3}}{(1+\mu_f)V_f(0)}\frac{1}{a_{exp}}\right) = 0 \Rightarrow a_{exp} = \frac{AP_{NH_3}}{(1+\mu_f)V_f(0)} \tag{17}$$

Therefore, the approximate solution at any time is presented in equation (18).

$$m_{TAN,f}(t) = m_{TAN,f}(0)exp\left(-\frac{AP_{NH_3}}{(1+\mu_f)V_f(0)}t\right) \tag{18}$$

When equation (18) is expressed in TAN concentration results in equation (19), which closely resembles the one obtained in the case where no water flux across the membrane occurs (equation (12)) (Serra-Toro et al., 2022a).

$$TAN_f(t) = \frac{m_{TAN,f}(t)}{V_f(t)} \approx \frac{m_{TAN,f}(t)}{V_f(0)} = TAN_f(0)exp\left(-\frac{AP_{NH_3}}{(1+\mu_f)V_f(0)}t\right) \tag{19}$$

Where $m_{TAN}(t)$ values are obtained by combining $TAN(t)$ and $V(t)$ experimental values.

2.6. Fitting procedure and graphical estimation

Membrane permeability (P_{NH_3}) was determined from experimental data using a non-linear regression approach. Model parameters were obtained by fitting an approximate analytical expression to the measured time series, using the Levenberg-Marquardt algorithm to minimise the reduced chi-squared statistic (χ^2_r), which accounts for the degrees of freedom of the fit. Parameter standard errors and goodness-of-fit metrics, including χ^2_r and the coefficient of determination (R^2), were computed to assess the quality of the calibration. Once P_{NH_3} was estimated, the model was used to predict dependent variables that could be directly compared with experimental observations. As an example, the mass balance for TAN in the trapping solution can be expressed as the time-dependent decrease in TAN mass in the feed compartment (equation (20)).

$$m_{TAN,t}(t) = m_{TAN,f}(0) - m_{TAN,f}(t) \tag{20}$$

To compare model predictions with experimental data on a concentration basis, TAN mass values in both compartments were converted to concentrations (g/L) by dividing them by the corresponding compartment volume at each time point (equation (21)).

$$TAN_f(t) = \frac{m_{TAN,f}(t)}{V_f(t)},\ TAN_t(t) = \frac{m_{TAN,t}(t)}{V_t(t)} \tag{21}$$

Since the compartment volumes were measured at discrete time points, smooth interpolating functions $V_f(t)$ and $V_t(t)$ were constructed to provide continuous volume estimates during the entire experiment. This procedure allowed a continuous representation of TAN concentration profiles, enabling direct graphical comparison between experimental measurements and model predictions. The resulting fitted curves and their corresponding R^2 values were then reported for all experimental datasets considered, allowing a comprehensive assessment of model performance. This approach was applied to reproduce the experimental TAN evolution of both solutions, which depend on their volume variation caused by water fluxes through the GPM, enabling the estimation of effective permeability and evaluating the model capability to capture volume variations. The predicted results obtained with the new model (namely, approximative model) were compared with those obtained from the model proposed by Da Silva et al. (2025), which incorporates osmotic pressure to describe water diffusion (namely, TAN-H_2O transport model). Additionally, comparison with the conventional constant-volume model highlights the influence of osmotic effects on the accuracy of TAN transport predictions.

3. Results and discussion

3.1. Water and ammonia diffusion using synthetic wastewater

Tests conducted at a volume relation of 2 (ω = 2) with synthetic wastewater were designed to demonstrate the increasing transport of water through the membrane as the TAN concentration in the trapping solution increased. The variation in the initial TAN concentration of the feed solution from 2.4 to 10.6 g N/L allowed the observation of a two-fold increase in the trapping solution concentration, which generated a water activity gradient between the two solutions. As this gradient intensified during the experiments, it promoted greater water transport through the membrane. In these experiments, both TAN concentration and volume were analysed and modelled using the approximative transport model developed in this study and compared with the TAN-H_2O transport model proposed by Da Silva et al. (2025) and the widely used constant-volume model (Serra-Toro et al., 2022b).

In Test A1.1, no water transport was observed since the concentration in the trapping solution reached 4.8 g N/L, which was insufficient to create a water activity gradient that promoted the diffusion of water through the membrane (Supplementary Material). The approximative transport model and TAN-H_20 transport model yielded P_{NH_3} of (1.76 ± 0.04)·10^{-6} and (2.48 ± 0.06)·10^{-6} m/s, respectively (Table 3). In contrast, Test A1.2 exhibited a small water flux of 0.09 L from the feed to the trapping solution after 50 h, leading to a slight dilution of the trapping solution concentration (Supplementary Material). Both models successfully predicted this effect with P_{NH_3} of (1.33 ± 0.06)·10^{-6} and (1.45 ± 0.07)·10^{-6} m/s, respectively. The TAN-H_2O transport model could not precisely estimate the water flux because of the small water transport; however, the permeability values were in accordance with the approximative model and concentration fitting data had R^2 higher than 0.98.

Fig. 1 shows the experimental and model data of Test A1.3. The TAN mass decrease in the feed solution matches the amount recovered in the trapping solution, indicating that no nitrogen losses occurred during the

Table 3
TAN permeabilities (P_{NH_3}) and water transport constants (K_w) for both models in experiments carried out with synthetic wastewater (Tests A1.1 – A2.4).

Test	Approximative model P_{NH3} (m/s · 10^{-6})	R^2	TAN-$H_2$0 transport model P_{NH3} (m/s · 10^{-6})	R^2	TAN-$H_2$0 transport model K_w (m/(s·bar) · 10^{-10})	R^2
A 1.1	1.76 ± 0.04	0.997	2.48 ± 0.06	0.997	–	–
A 1.2	1.33 ± 0.06	0.987	1.45 ± 0.07	0.986	–	–
A 1.3	1.31 ± 0.02	0.998	1.49 ± 0.04	0.998	4.8 ± 0.7	0.816
A 1.4	0.69 ± 0.02	0.996	0.76 ± 0.04	0.995	11 ± 3	0.842
A 2.1	1.72 ± 0.04	0.996	2.06 ± 0.09	0.997	8.2 ± 0.3	0.989
A 2.2	1.05 ± 0.03	0.996	1.20 ± 0.04	0.996	3.4 ± 0.2	0.946
A 2.3	0.92 ± 0.02	0.996	1.17 ± 0.07	0.995	2.4 ± 0.1	0.964
A 2.4	1.21 ± 0.03	0.995	1.57 ± 0.09	0.996	2.8 ± 0.1	0.993
Distribution (x ± s)	1.3 ± 0.4	–	1.4 ± 0.4	–	5.5 ± 3.5	–

experiment. During the first 3 h, a slight water flux toward the feed solution was detected, likely due to the high NH_4Cl concentration (7.5 g N/L). However, the trend soon reversed with water starting to migrate toward the trapping solution, where osmotic pressure increased as $(NH_4)_2SO_4$ accumulated due to TAN transfer. These fluxes were driven by the activity gradient between both solutions, with water migrating toward the solution with the higher concentration of dissolved species. The net water transferred was 0.21 L after 50 h of operation.

The new model approach (equation (19)) accurately predicted TAN concentrations in both solutions. P_{NH_3} values of $1.31{\cdot}10^{-6}$ and $1.49{\cdot}10^{-6}$ m/s were obtained from the fitted TAN concentrations for the approximative and TAN-H_2O transport models, respectively (Table 3). These results are highly consistent between models and aligned with values reported in literature using GPM contactors for nitrogen recovery from synthetic solutions (Serra-Toro et al., 2022a; Yan et al., 2023; Abeyratne et al., 2025). Both TAN models exhibited an excellent predictive performance, with R^2 values above 0.99 (Table 3). It is worth mentioning that this approach makes it possible to quantify the TAN concentration decrease attributable to dilution effects, an aspect not accounted for by the traditional models that consider constant volumes. The divergence between the ammonia mass transfer coefficient (K_m) obtained by the constant-volume model and the new model is illustrated in the Supplementary Material. These results clearly show the importance of accounting for water fluxes under high osmotic pressure gradients, especially when designing and optimising GPM contactors for nitrogen recovery from high-strength effluents.

The volume transfer in Test A1.4 was higher than in the previous tests due to the higher initial TAN concentration of 10.5 g N/L. Fig. 2 shows that during the first 5 h of operation, water migrated toward the feed solution until the osmotic pressure in the trapping solution surpassed that of the feed, at which point the water flux changed towards the trapping solution. After 50 h, a total net water exchange of 0.42 L was measured, twice the amount observed in Test A1.3, where the osmotic pressure gradient was lower. The TAN-H_2O transport model slightly overestimated water transport, but it still provided a robust prediction of the overall trend and accurately estimated TAN concentrations. The P_{NH_3} was $0.69{\cdot}10^{-6}$ and $0.76{\cdot}10^{-6}$ m/s for the approximative and TAN-H_2O transport model, respectively (Table 3). As in Test

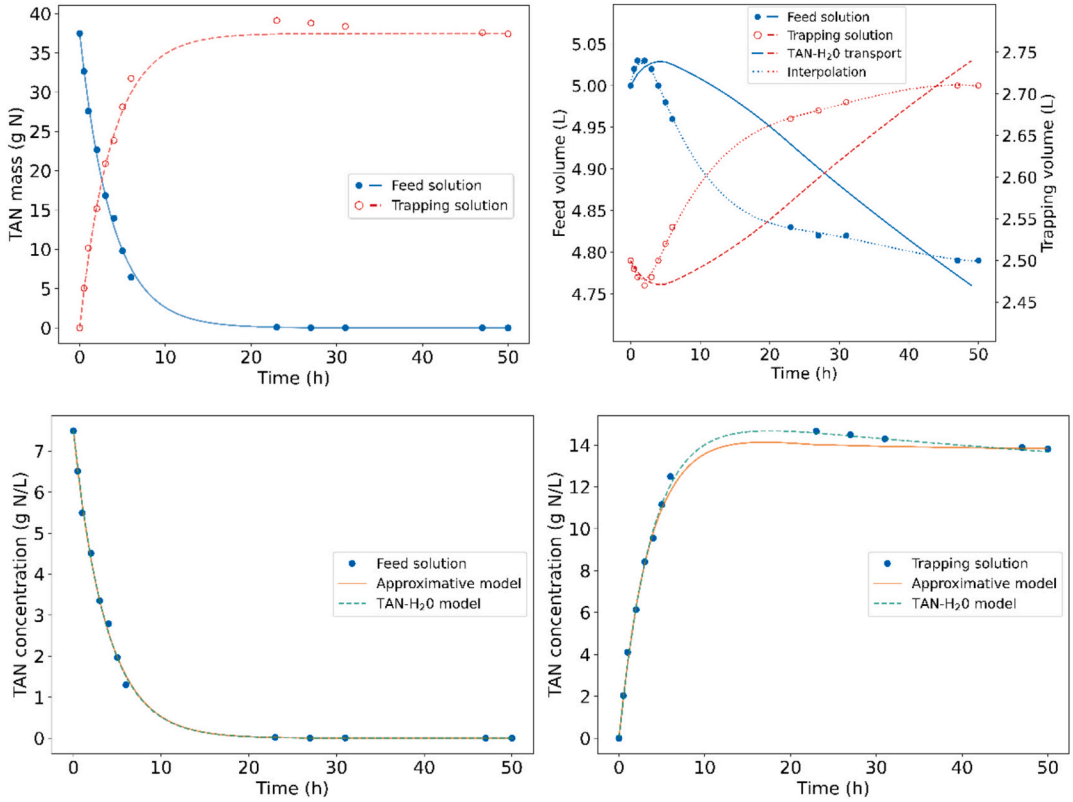

Fig. 1. Experiment carried out with a synthetic solution at 7.5 g N/L and ω of 2 (Test A1.3). TAN mass evolution (top left), volume evolution (top right) for both solutions, feed concentration adjustment (bottom left) and trapping concentration adjustment (bottom right). Dots represent experimental data, and lines represent model fitting.

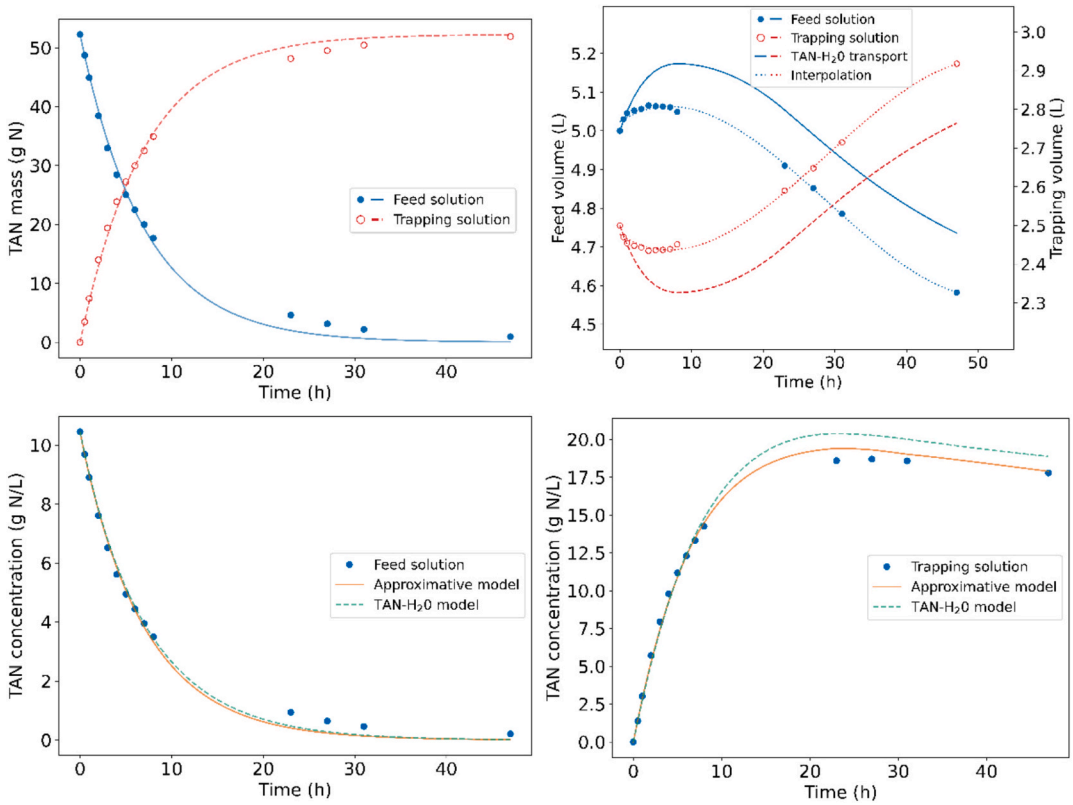

Fig. 2. Experiment carried out with a synthetic solution at 10.2 g N/L and ω of 2 (Test A1.4). TAN mass evolution (top left), volume evolution (top right) for both solutions, feed concentration adjustment (bottom left) and trapping concentration adjustment (bottom right). Dots represent experimental data, and lines represent model fitting.

A1.3, model fitting in the feed solution was excellent since the water flux had negligible impact once TAN concentration approached zero. For the trapping solution, the approximative model yielded a slightly better fit although both models reached R^2 above 0.995. This assay showed a greater divergence between the P_{NH_3} and the literature K_m fit since higher amount of water diffused through the membrane (see Supplementary Material).

Table 3 summarises the P_{NH_3} values obtained with the approximative and the TAN-H_2O transport models, together with the corresponding R^2 for all synthetic solution assays (Tests A1.1 – A2.4). For the approximative model, permeability values were very consistent, with a mean of $(1.3 \pm 0.4)\cdot10^{-6}$ m/s. This narrow distribution confirms the robustness of the model, as permeability is a membrane-intrinsic parameter and, therefore, should be independent of TAN concentration or volume ratio. The K_w values from the TAN-H_2O transport were comparable across all tests working with synthetic wastewater (excluding Tests A1.1 and A1.2 due to a low water transport), averaging $(3.7 \pm 2.3)\cdot10^{-10}$ m/(s·bar). The P_{NH_3} observed for the TAN-H_2O transport model had a mean value of $(1.4 \pm 0.4)\cdot10^{-6}$ m/s, showing a similar behaviour to that of the approximative model and further supporting the consistency of the results.

Overall, both the approximative transport model proposed in this study and the previously published TAN-H_2O transport model (Da Silva et al., 2025) provided an excellent fit to the experimental data obtained with synthetic solutions, with consistently high R^2 values. This indicates that under controlled conditions both approaches are able to accurately reproduce the dilution effects caused by water transport across the membrane. These results confirm that the simplified modelling framework can reliably describe ammonia and water transport when the composition of the system is well defined. In this research, the experiments with synthetic solutions mainly served as a validation step to assess the consistency of the simplified model regarding the previously established TAN-H_2O transport model. Once this agreement was confirmed, the modelling approach was applied to real wastewater matrices to evaluate its performance under more complex and variable conditions. Real wastewaters present a heterogeneous and variable composition, which makes the estimation of osmotic pressure challenging from a practical perspective. Therefore, avoiding the need to estimate these parameters represents a key advantage of the modelling approach proposed in this work.

3.2. *Water and ammonia diffusion using waste-derived streams*

The experiments conducted with supernatant from an OFMSW anaerobic digester, which had an initial TAN concentration of 5.7 g N/L, lasted 72 and 96 h for the experiment with a ω of 2 and 10, respectively. In the case of operating with a volume relation of 2 (Test B1), a slight water flux toward the feed solution was observed during the first 8 h. No further water transport was observed as confirmed by the final TAN concentration in the trapping solution that reached twice the concentration of the feed solution after approximately 25 h. Considering the high conductivity of the AD supernatant (50.6 mS/cm), the osmotic pressure difference between the feed and the trapping solution enriched with $(NH_4)_2SO_4$ was smaller than in the experiments using synthetic wastewater. When using waste-derived effluents, the K_w in the experiments cannot be calculated since osmotic pressure is too difficult to estimate (Khraisheh et al., 2020). Therefore, a monitoring of the volume was carried out to determine the P_{NH_3}, which value was $(0.92 \pm 0.03)\cdot10^{-6}$ m/s ($R^2 = 0.994$) (Table 4). This value is slightly lower than that obtained in synthetic experiments, which is attributed to the species interactions in the complex solution matrix.

A higher water flux was observed in Test B2, where the volume relation was 10. The maximum TAN concentration in the trapping solution was approximately 35 g N/L, much lower than the theoretical 56

Table 4
TAN permeabilities (P_{NH3}) of the approximative model in tests carried out with waste-derived effluents (Tests B, C and D).

Test	P_{NH3} (m/s · 10^{-6})	R^2
B1	0.90 ± 0.03	0.994
B2	0.88 ± 0.06	0.967
C1	0.58 ± 0.03	0.987
C2	0.77 ± 0.04	0.976
D	1.83 ± 0.09	0.986

g N/L expected in the absence of water transport. After about 10 h, the TAN concentration started to decrease gradually, and by 96 h a net water transfer of 0.97 L to the trapping solution had occurred, driven by the high osmotic pressure generated by the ammonium salt content (Fig. 3). These results indicate that higher osmotic pressure gradients increase water transport, suggesting that osmotic distillation is the main mechanism. However, the contribution of membrane wetting to water transport cannot be excluded (Zhang et al., 2025). The P_{NH_3} was (0.88 ± 0.06)·10^{-6} m/s (R^2 = 0.97), coinciding with that obtained in Test B1. A noticeable divergence occurs when estimating the permeability of ammonia without considering the water diffusion when the trapping solution is highly concentrated (Supplementary Material).

Similarly, the experiment performed with OFMSW fermentation liquid and a volume relation of 2 (Test C1) showed water transport only towards the feed solution during the first hours of operation, with no detectable water flux thereafter. This behaviour is illustrated in Fig. 4, where TAN concentration in the trapping solution remained nearly constant after 30 h of operation. A slight decrease in the trapping solution volume could also be inferred since the final concentration reached 13.9 g N/L, whereas under constant-volume conditions it would have been 12.6 g N/L, doubling the initial feed concentration of 6.3 g N/L. The P_{NH_3} was (0.58 ± 0.03)·10^{-6} m/s (R^2 = 0.99), very similar to previous tests carried out with OFMSW anaerobic digestion supernatant (Tests B1 and B2) since effluent characteristics were resemblant (Table 1).

In experiments with OFMSW fermentation liquid and a volume relation of 10 (Test C2), dilution effects during the first 15 h were even more remarkable than those using the AD supernatant. The maximum TAN concentration reached was nearly 30 g N/L instead of the theoretical 60 g N/L expected in the absence of water transport. The final TAN concentration of 24.9 g N/L was consistent with a total net water exchange of 0.67 L over 96 h of operation. In Test C2, the P_{NH_3} had a value of (0.77 ± 0.03)·10^{-6} m/s (R^2 = 0.98) similar to the one obtained in previous tests performed with high strength wastewaters (Table 4). This value substantially differs from the constant-volume K_m that predicts a double concentration in the trapping solution (Supplementary Material).

The ABP wastewater was the effluent that exhibited the highest conductivity of 57.9 mS/cm, consistent with its content of dissolved species such as TAN (9.9 g N/L) and VFA (65.1 g COD/L), among others (Table 4). This high ionic content was directly related to water activity and, consequently, to osmotic pressure, creating a strong gradient at the start of the experiment towards the ABP feed solution (Fig. 5). As a result, Test D (ω of 5) initially showed a net water flux towards the feed solution, leading to a decrease in the trapping solution volume and a TAN concentration of 60 g N/L. However, this concentration subsequently declined, as the large amount of $(NH_4)_2SO_4$ in the trapping solution eventually caused the trapping solution to reach a higher osmotic pressure than the feed. The resulting P_{NH_3} was notably higher than in previous tests, with a value of (1.83 ± 0.09)·10^{-6} m/s (R^2 = 0.99). This value was more than two times higher than values in Tests B and C, probably due to the different matrix and the interaction of their species. The permeability parameter successfully captured both the over-concentration and under-concentration phases in the trapping solution, whereas the traditional K_m approach estimated only an intermediate value (Supplementary Material).

It is also worth noting that an additional test using ABP wastewater at a volume relation of 2 was discarded, as the trapping solution lost too much volume to allow precise monitoring. This occurred because the $(NH_4)_2SO_4$ concentration was insufficient to balance the water activities of the two solutions and halt the water flux. Along all waste-derived effluent tests no significant decrease in permeability values was

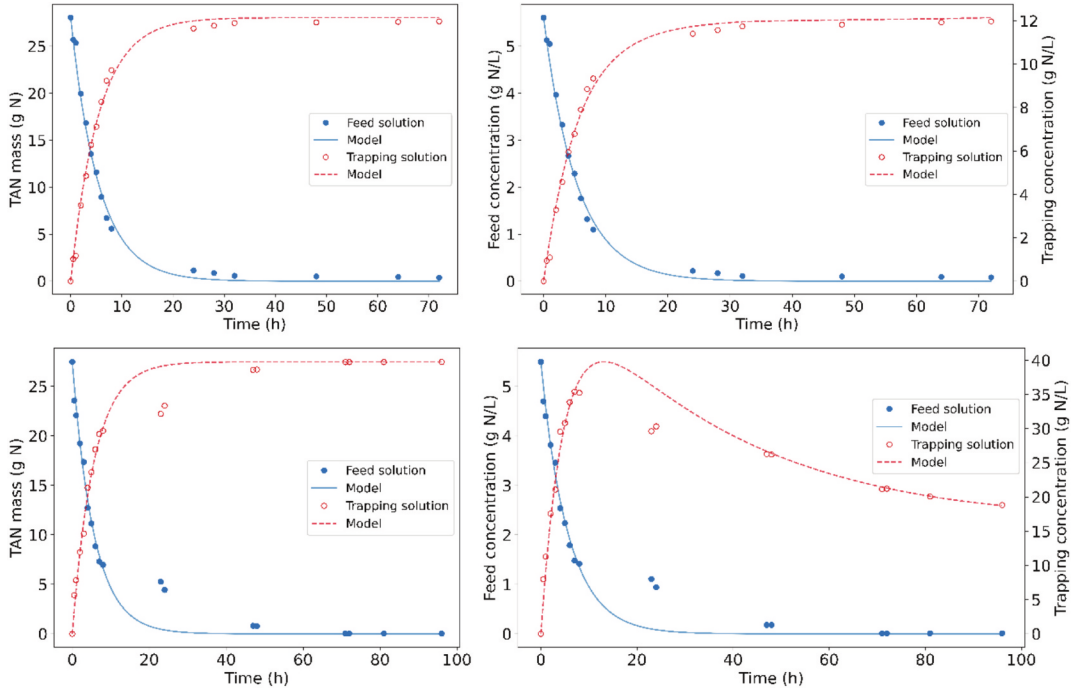

Fig. 3. Experiments carried out with OFMSW anaerobic digestion supernatant. TAN evolution in mass (top left) and concentration (top right) for the experiments with ω of 2 (Test B1), and TAN evolution in mass (bottom left) and concentration (bottom right) for the experiments with ω of 10 (Test B2). Dots represent experimental data, and lines represent model fitting of the approximative model.

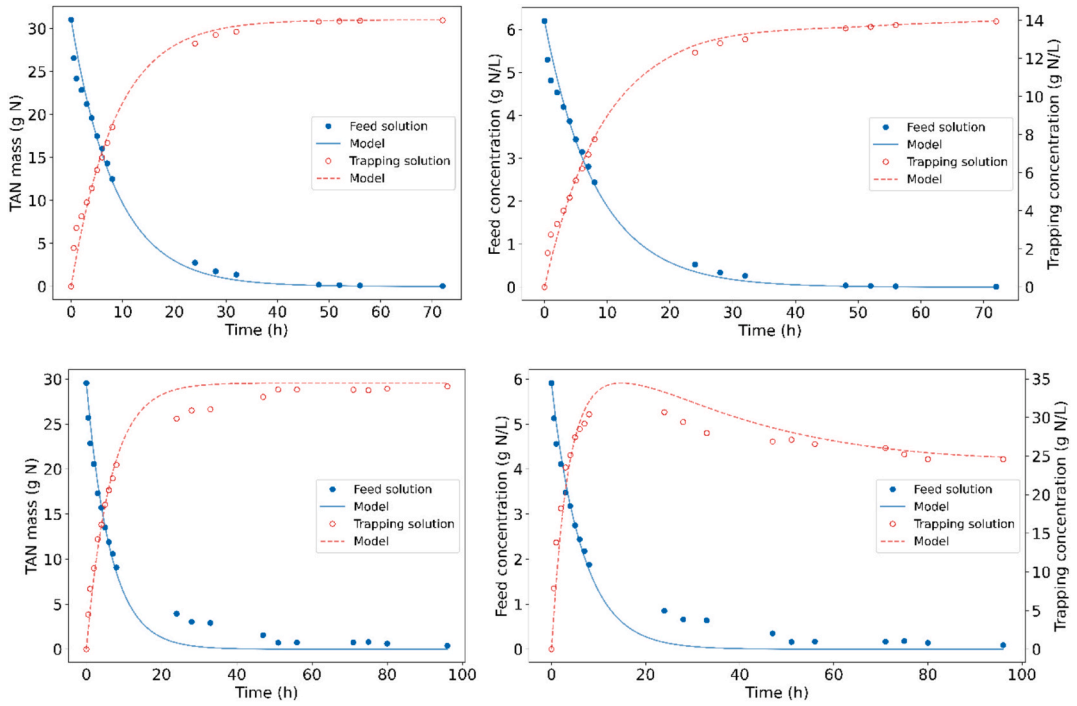

Fig. 4. Experiments carried out with OFMSW fermentation liquid. TAN evolution in mass (top left) and concentration (top right) for the experiment with a ω of 2 (Test C1), and TAN evolution in mass (bottom left) and concentration (bottom right) for the experiment with a ω of 10 (Test *C*2). Dots represent experimental data, and lines represent model fitting of the approximative model.

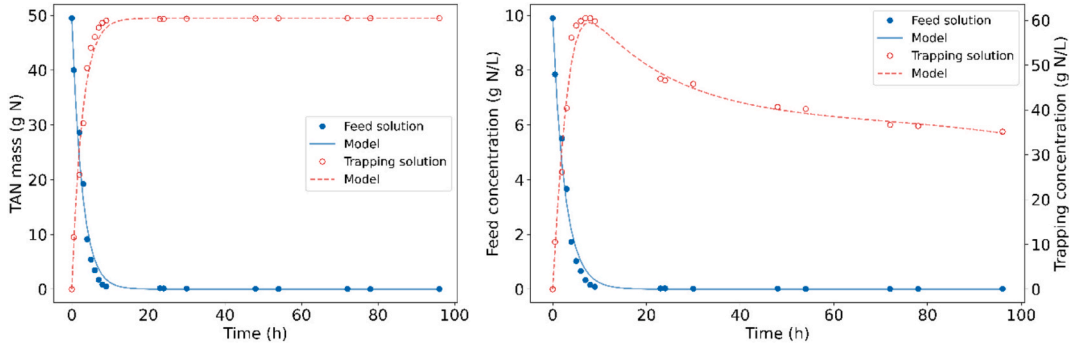

Fig. 5. Experiments carried out with ABP wastewater. TAN evolution in mass (left) and concentration (right) for the experiment with ω of 5 (Test C). Dots represent experimental data, and lines represent model fitting of the approximative model.

observed across the experimental replicates, suggesting that fouling did not have a noticeable impact over the time scale of this study experiments. Further research is needed to elucidate the implications of extremely high water transport and the wetting propensity of GPM when treating high-strength effluents, as well as to better understand their impact on long-term performance (Aligwe et al., 2020).

4. Conclusions

A new modelling framework capable of describing the coupled transport of ammonia and water across gas-permeable membranes (GPM) using only experimentally measurable variables have been developed and validated. The model successfully reproduced the evolution of TAN concentrations for both synthetic solutions and waste-derived effluents. The permeability values obtained for synthetic solutions were highly consistent, with a mean value of $(1.3 \pm 0.4)\cdot10^{-6}$ m/s, confirming that ammonia permeability behaves as an intrinsic membrane parameter. When applied to waste-derived effluents, the model was also able to capture dilution effects caused by water transport across the membrane, which significantly influenced trapping solution concentrations. These results highlight a key limitation of conventional modelling approaches that rely on osmotic pressure estimations or constant-volume assumptions, which are difficult to apply to real wastewater matrices due to their complex and variable composition. The modelling strategy proposed here addresses this gap by enabling the interpretation of ammonia and water transport without requiring detailed thermodynamic characterisation. Overall, this approach provides a practical tool to analyse GPM performance under realistic conditions and contributes to improving the interpretation and design of GPM nitrogen recovery systems.

Ethical approval

Not applicable.

CRediT authorship contribution statement

A. Serra-Toro: Writing – original draft, Methodology, Investigation,

Formal analysis, Data curation. **T. Romero-Vidal:** Writing – original draft, Investigation, Formal analysis, Data curation. **V. Pelizzaro:** Methodology, Investigation, Formal analysis. **C. Da Silva:** Writing – original draft, Formal analysis, Data curation. **F. Valentino:** Writing – review & editing, Supervision, Conceptualization. **S. Astals:** Writing – review & editing, Supervision, Funding acquisition, Conceptualization. **J. Dosta:** Writing – review & editing, Supervision, Methodology, Formal analysis, Data curation, Conceptualization. **F. Mas:** Writing – review & editing, Supervision, Methodology, Formal analysis, Data curation, Conceptualization.

Declaration of competing interest

The authors declare that they have no known competing financial interests or personal relationships that could have appeared to influence the work reported in this paper.

Acknowledgements

This work is supported by the Spanish Ministry of Science, Innovation and Universities (TED2021-132422B-I00 and PID2022-142023OB-I00). A. Serra-Toro is grateful to the Spanish Ministry of Science, Innovation and Universities for his FPI grant (PREP2022-000850). C. Da Silva is grateful to Agència de Gestió d'Ajuts Universitaris i de Recerca (AGAUR) de Catalunya for his predoctoral grant (2020 FISDUR 00554). The authors also wish to thank the Institut de l'Aigua of University of Barcelona for their financial support. F. Mas and T. Romero-Vidal acknowledge the financial support of the Spanish Structures of Excellence Maria de Maeztu program (CEX2021-001202-M). The authors would like to thank the Catalan Government for the quality accreditation given to both research groups of the University of Barcelona (2021 SGR 00234 and 2021 SGR 00350).

Appendix A. Supplementary data

Supplementary data to this article can be found online at https://doi.org/10.1016/j.biortech.2026.134711.

Data availability

Data will be made available on request.

References

Abeyratne, W.M.L.K., Munasinghe Arachchige, S.P., Bayat, H., Zhang, Y., Brewer, C.E., Nirmalakhandan, N., 2025. Gas permeable membrane technology for nitrogen fertilizer recovery from nitrogen-rich waste streams. J. Water Process Eng. 75, 108064. https://doi.org/10.1016/j.jwpe.2025.108064.

Aligwe, P.A., Sirkar, K.K., Canlas, C.J., Cheng, W.C., 2020. Supported gas membrane-based ammonia removal and recovery for a pH-dependent sink: effect of water vapor transport. J. Membr. Sci. 611, 118308. https://doi.org/10.1016/j.memsci.2020.118308.

APHA, 2017. Standard Methods for the Examination of Water and Wastewater, 23rd ed. American Public Health Association, Washington DC.

Chan, Z.P., Li, L., Kang, G., Manan, N.A., Cao, Y., Wang, T., 2020. Discussion on Water Condensation in Membrane Pores during CO_2 Absorption at High Temperature. Membranes 10 (12), 407. https://doi.org/10.3390/membranes10120407.

Darestani, M., Haigh, V., Couperthwaite, S.J., Millar, G.J., Nghiem, L.D., 2017. Hollow fibre membrane contactors for ammonia recovery: current status and future developments. J. Environ. Chem. Eng. 5 (2), 1349–1359. https://doi.org/10.1016/j.jece.2017.02.016.

Da Silva, C., Serra-Toro, A., Pelizzaro, V., Valentino, F., Astals, S., Mas, F., Dosta, J., 2025. Modeling nitrogen recovery and water transport in gas-permeable membranes. Water Res. 269, 122771. https://doi.org/10.1016/j.watres.2024.122771.

Errico, M., Sotoft, L.F., Nielsen, A.K., Norddahl, B., 2018. Treatment costs of ammonia recovery from biogas digestate by air stripping analyzed by process simulation. Clean Techn. Environ. Policy 20, 1479–1489. https://doi.org/10.1007/s10098-017-1468-0.

Farghali, M., Chen, Z., Osman, A.I., Ali, I.M., Hassan, D., Ihara, I., Rooney, D.W., Yap, P. S., 2024. Strategies for ammonia recovery from wastewater: a review. Environ. Chem. Lett. 22, 2699–2751. https://doi.org/10.1007/s10311-024-01768-6.

Ferri da Silva, J.F., Tápparo, D.C., Lazaroto, A.C., de Asis, D.B., Sophiatti, I.V.M., Magrini, F.E., Steinmetz, R.L.R., Antes, F.B., Vanotti, M., Paesi, S., Kunz, A., 2025. Enhancing anaerobic digestion of nitrogen-rich substrates through in situ ammonia recovery using tubular gas-permeable membranes. Bioresour. Technol. 437, 133063. https://doi.org/10.1016/j.biortech.2025.133063.

Fowler, D., Coyle, M., Skiba, U., Sutton, M.A., Cape, J.N., Reis, S., Sheppard, L.J., Jenkins, A., Grizzetti, B., Galloway, J.N., Vitousek, P., Leach, A., Bouwman, A.F., Butterbach-Bahl, K., Dentener, F., Stevenson, D., Amann, M., Voss, M., 2013. The global nitrogen cycle in the twenty-first century. Philos. Trans. R. Soc. B 368 (1621), 1471–2970. https://doi.org/10.1098/rstb.2013.0164.

García-González, M.C, Vanotti, M.B., 2015. Recovery of ammonia from swine manure using gas-permeable membranes: Effect of waste strength and pH. Waste Management. Volume 38, April 2015, Pages 455-461. doi: 10.1016/j.wasman.2015.01.021.

González-García, I., Riaño, B., Molinuevo-Salces, B., Vanotti, M.B., García-González, M. C., 2021. Improved anaerobic digestion of swine manure by simultaneous ammonia recovery using gas-permeable membranes. Water Research 190, 116789. https://doi.org/10.1016/j.watres.2020.116789.

Greisner, B., Mauer, D., Rögener, F., Lerch, A., 2023. Predicting Water Flux in Forward Osmosis with unknown Feed solution Composition: an Empirical Approach based on Thermodynamical Properties. Membranes 13, 427. https://doi.org/10.3390/membranes13040427.

Guo, G., Li, Y., Zhou, S., Chen, Y., Urasaki, K., Qin, Y., Kubota, K., Li, Y.Y., 2022. Long term operation performance and membrane fouling mechanisms of anaerobic membrane bioreactor treating waste activated sludge at high solid concentration and high flux. Sci. Total Environ. 846, 157435. https://doi.org/10.1016/j.scitotenv.2022.157435.

Karmann, C., Mágrová, A., Jeníček, P., Bartáček, J., Kouba, V., 2024. Advances in nitrogen removal and recovery technologies from reject water: Economic and environmental perspectives. Bioresource Technology. Volume 391, Part A, January 2024, 129888. doi: 10.1016/j.biortech.2023.129888.

Khraisheh, M., Dawas, N., Nasser, M.S., Al-Marri, M.J., Hussien, M.A., Adham, S., McKay, G., 2020. Osmotic pressure estimation using the Pitzer equation for forward osmosis modelling. Environ. Technol. 41 (19), 2533–2545. https://doi.org/10.1080/09593330.2019.1575476.

Ladewig, B., Al-Shaeli, M.N.Z., 2017. Fundamentals of membrane bioreactors. Fundamentals of Membrane Bioreactors. Materials, Systems and Membrane Fouling. 10.1007/978-981-10-2014-8.

Ledezma, P., Kuntke, P., Buisman, C.J.N., Keller, J., Freguia, S., 2015. Source-separated urine opens golden opportunities for microbial electrochemical technologies. Trends in Biotechnology 33 (4), 214–220. https://doi.org/10.1016/j.tibtech.2015.01.007.

Lee, W., An, S., Choi, Y., 2021. Ammonia harvesting via membrane gas extraction at moderately alkaline pH: A step toward net-profitable nitrogen recovery from domestic wastewater. Chemical Engineering Journal. Volume 405, 1 February 2021, 126662. doi: 10.1016/j.cej.2020.126662.

Nagy, J., Kaljunen, J., Toth, A.J., 2019. Nitrogen recovery from wastewater and human urine with hydrophobic gas separation membrane: experiments and modelling. Chem. Pap. 73, 1903–1915. https://doi.org/10.1007/s11696-019-00740-x.

Nancharaiah, Y.V., Mohan, S.V., Lens, P.N.L., 2016. Recent advances in nutrient removal and recovery in biological and bioelectrochemical systems. Bioresource Technology 215, 173–185. https://doi.org/10.1016/j.biortech.2016.03.129.

Qin, Y., Wang, K., Xia, Q., Yu, S., Zhang, M., An, Y., Zhao, X., Zhou, Z., 2023. Up-concentration of nitrogen from domestic wastewater: a sustainable strategy from removal to recovery. Chemical Engineering Journal. Volume 451, Part 3, 138789. https://doi.org/10.1016/j.cej.2022.138789.

Reig, M., Vecino, X., Gibert, O., Valderrama, C., Cortina, J.L., 2021. Study of the operational parameters in the hollow fibre liquid-liquid membrane contactors process for ammonia valorisation as liquid fertiliser. Sep. Purif. Technol. 255, 117768. https://doi.org/10.1016/j.seppur.2020.117768.

Rizzioli, F., Bertasini, D., Bolzonella, D., Frison, N., Battista, F., 2023. A critical review on the techno-economic feasibility of nutrients recovery from anaerobic digestate in the agricultural sector. Separation and Purification Technology. Volume 306, Part B, 122690. doi: 10.1016/j.seppur.2022.122690.

Rongwong, W., Sairiam, S., 2020. A modeling study on the effects of pH and partial wetting on the removal of ammonia nitrogen from wastewater by membrane contactors. J. Environ. Chem. Eng. 8, 104240. https://doi.org/10.1016/j.jece.2020.104240.

Rosa e Silva, G.O., Rodrigues dos Santos, C., Souza Casella, G., Pinheiro Drumond, G., Santos Amaral, M.C., 2025. Membrane fouling in integrated forward osmosis and membrane distillation systems – A review. Separation and Purification Technology. 356, Part B, 129955. doi: 10.1016/j.seppur.2024.129955.

Serra-Toro, A., Astals, S., Madurga, S., Mata-Álvarez, J., Mas, F., Dosta, J., 2022. Ammoniacal nitrogen recovery from pig slurry using a novel hydrophobic/hydrophilic selective membrane. J. Environ. Chem. Eng. 10 (5), 108434. https://doi.org/10.1016/j.jece.2022.108434.

Serra-Toro, A., Vinardell, S., Astals, S., Madurga, S., Llorens, J., Mata-Álvarez, J., Mas, F., Dosta, J., 2022. Ammonia recovery from acidogenic fermentation effluents using a gas-permeable membrane contactor. Bioresour. Technol. 356, 127273. https://doi.org/10.1016/j.biortech.2022.127273.

Serra-Toro, A., Ben Hammou Abboud, Y., Cardete-Garcia, M. A., Astals, S., Valentino, F., Mas, F., Dosta, J., 2024. Ammoniacal nitrogen recovery from swine slurry using a gas-permeable membrane: pH control strategies and feed-to-trapping volume ratio. Environmental Science and Pollution Research. doi: 10.1007/s11356-024-32193-5.

Serra-Toro, A., Abad, E., Peña-Picola, S., Valentino, F., Fernández, I., Astals, S., Dosta, J., 2025. Upcycling fermentation liquors by integrating membrane contactors for

nitrogen recovery and forward osmosis for volatile fatty acids up-concentration. J. Environ. Manage. 389, 126044. https://doi.org/10.1016/j.jenvman.2025.126044.

Soto-Herranz, M., Sánchez-Báscones, M., Antolín-Rodríguez, J. M., Martín-Ramos, P., 2022. Evaluation of Different Capture Solutions for Ammonia Recovery in Suspended Gas Permeable Membrane Systems. Membranes. 12(6), 572; doi: 10.3390/membranes12060572.

Varela-Corredor, F., Bandini, S., 2020. Testing the applicability limits of a membrane distillation process with ceramic hydrophobized membranes: The critical wetting temperature. Separation and Purification Technology. Volume 250, 1 November 2020, 117205. doi: 10.1016/j.seppur.2020.117205.

Wong, P.W., Yim, V.M.W., Guo, J., Chan, B.S., Deka, B.J., Na, A.K., 2021. Noninvasive Real-Time monitoring of Wetting Progression in Membrane Distillation using Impedance Spectroscopy. Environ. Sci. Tech. 56 (1), 535–545. https://doi.org/10.1021/acs.est.1c04433.

Wu, L., Xiu, Y., Shen, Z., Zhou, Y., Zuo, J., 2026. Integrated digestate concentration, ammonia recovery, and water reclamation via a novel two-stage submerged gas-permeable membrane system. J. Membr. Sci. 740, 124920. https://doi.org/10.1016/j.memsci.2025.124920.

Yan, X., He, L., Zhang, W., Chen, W., Wu, J., Yang, N., Cai, X., Li, L., Yan, L., Rao, P., 2023. Efficient ammonia-nitrogen removal and recovery from wastewater via the continuous flat-sheet gas-permeable membranes reactor pretreatment. J. Water Process Eng. 52, 103571. https://doi.org/10.1016/j.jwpe.2023.103571.

Ye, Y., Ngo, H.H., Guo, W., Liu, Y., Chang, S.W., Nguyen, D.C., Liang, H., Wang, J., 2018. A critical review on ammonium recovery from wastewater for sustainable wastewater management. Bioresource Technology 268, 749–758. https://doi.org/10.1016/j.biortech.2018.07.111.

Zhang, H., Yu, H., Wang, Z., Qing, Y., Han, M., Ye, J., Han, L., 2025. Hierarchical-Porous Gas-Permeable Membrane toward Efficient and Robust Ammonia Recovery. Environ. Sci. Technol. 60 (3), 2742–2751. https://doi.org/10.1021/acs.est.5c10757.

Zhu, Y., Chang, H., Yan, Z., Liu, C., Liang, Y., Qu, F., Liang, H., Vidic, R.D., 2024. Review of ammonia recovery and removal from wastewater using hydrophobic membrane distillation and membrane contactor. Separation and Purification Technology. Volume 328, 1 January 2024, 125094. doi: 10.1016/j.seppur.2023.125094.